

A first estimate of the NNLO nonresonant corrections to top-antitop threshold production at lepton colliders

Pedro Ruiz-Femenía

Instituto de Física Corpuscular (IFIC), CSIC-Universitat de València, E-46980 Paterna, Spain

(Dated: February 6, 2014)

We compute the dominant term in the expansion in $\rho = 1 - M_W/m_t$ of the unknown next-to-next-to-leading order (NNLO) nonresonant contributions to the $e^+e^- \rightarrow W^+W^-b\bar{b}$ total cross section at energies close to the top-antitop threshold. Our analytic result disagrees with a previous calculation by other authors [1]. We show that our determination has the correct infrared structure needed to cancel the divergences proportional to the top width arising in the resonant production of the same final state, and we point out to a missing contribution in the computation of [1] to explain the discrepancy.

I. INTRODUCTION

Stringent tests of the electroweak symmetry breaking sector of the Standard Model shall require a very precise knowledge of the top-quark properties, and most crucially of its mass. The measurement of the top-antitop production cross section line shape at a future e^+e^- collider could allow us to determine the top mass with an uncertainty below 100 MeV [2] which is beyond the reach of hadronic colliders. Substantial effort has been put in the past to increase the accuracy in the calculation of the $e^+e^- \rightarrow t\bar{t}$ cross section with the use of perturbative methods that include all-order resummations of QCD corrections in the threshold region. The latter arise from Coulomb-gluon exchange between the top and the antitop that are produced nearly on-shell (resonantly), and are responsible for the characteristic $t\bar{t}$ threshold line shape, where a remnant of a toponium 1S resonance, smoothed out by the large top width ($\Gamma_t \approx 1.5$ GeV), is visible. For a long time, the aim was put in the calculation of the resonant QCD corrections with the help of the non-relativistic effective field theory of QCD (NRQCD): within the power counting defined by $v \sim \alpha_s$, with v the relative velocity of the top and antitop, next-to-next-to-leading logarithmic (NNLL) and fixed-order N³LO results have become available (for the most recent calculations concerning the resonant pieces see [3–5]).

The high accuracy reached in the evaluation of QCD corrections has also called for an assessment of the electroweak corrections and higher-order effects related to the top-quark instability. In the resonant side, the top decay is simply accounted for at leading order by including the top width in the NRQCD top-antitop propagator, $(E - \mathbf{p}^2/m_t + i\Gamma_t)^{-1}$, which enforces the counting $\Gamma_t \sim m_tv^2 \sim m_t\alpha_s^2$, or equivalently, $\alpha_{\text{EW}} \sim \alpha_s^2$. Beyond leading order, apart from subleading resonant electroweak effects [6], we have to consider the possibility that the physical final state, $W^+W^-b\bar{b}$ (treating W bosons as stable) is produced

non-resonantly, *i.e.* by processes that do not involve a nearly on-shell $t\bar{t}$ pair. The leading nonresonant effects are NLO for the cross section and account for the full-theory contributions where one of the bW pairs is produced from an on-shell top, while the other pair emerges from a highly virtual top or directly without an intermediate top. They were calculated in [7], and shown to yield a constant negative shift of order 3% with respect the LO (resonant) result above threshold and to become particularly relevant below, where the resonant contributions rapidly vanish. At NNLO, the nonresonant corrections arise from attaching real and virtual gluons to the NLO diagrams. They are only known when cuts on the invariant masses on the bW pairs of size Λ^2 , with $m_t\Gamma_t \ll \Lambda^2 \ll m_t^2$, are applied [8, 9]. The extrapolation of the results of the latter works for the total cross section case, $\Lambda_{\text{max}}^2 = m_t^2 - M_W^2$, suggests that the NNLO contributions are only one half smaller than the NLO ones. Given that the simulation studies of a $t\bar{t}$ threshold scan at a future e^+e^- collider are able to identify top pair events with high purity without applying cuts on the top and antitop invariant masses, a calculation of the NNLO nonresonant effects for the totally inclusive cross section will become necessary in order to reach a percent accuracy in the theory input.

In this note we provide an approximation to the NNLO nonresonant total cross section by performing an expansion in the parameter $\rho = 1 - M_W/m_t$. This expansion was applied in [1] to determine the NLO nonresonant contributions up to very high orders in ρ , confirming the results from [7]. Despite the fact that ρ is not a small parameter at its physical value ($\rho \approx 0.5$), it was found in [1] that the dominant term in this expansion gives a result that differs from the exact one by only 5%. Ref. [1] also provided the leading and subleading pieces in ρ for the NNLO corrections, scaling as ρ^{-1} and $\rho^{-1/2}$, respectively. However, as pointed out in [9], the infrared divergent part of the NNLO ρ^{-1} term given in [1] does not match

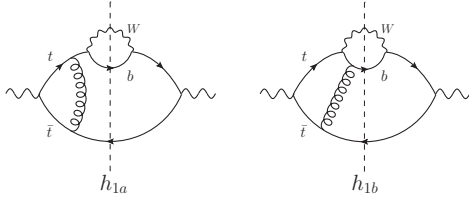


FIG. 1. $\mathcal{O}(\alpha_s)$ corrections to the two-loop forward-scattering diagrams which provide the $\mathcal{O}(\rho^{-1})$ NNLO non-resonant approximation. The e^+e^- external legs have not been drawn. The symmetric diagrams with the gluon in the r.h.s of the cut, or with $\bar{b}W^-t$ cuts are not shown.

the structure needed to cancel the well-known finite-width divergences $\propto \frac{\alpha_s \Gamma_t}{\epsilon}$ that arise in the NNLO resonant cross section at the same order in ρ . Such cancellation is mandatory since the full-theory calculation for the same process is finite [10] (see also [11]). This mismatch is corrected in this work by providing a new evaluation of the ρ^{-1} term which yields the correct infrared structure, and that can be combined with the NNLO resonant corrections in a regularization-scheme independent way.

II. NNLO NONRESONANT CROSS SECTION: EXPANSION IN $\rho = 1 - M_W/m_t$

The total $e^+e^- \rightarrow W^+W^-b\bar{b}$ cross section is conveniently obtained by extracting the cuts of the e^+e^- forward-scattering amplitude related to this final state. The separation of resonant and nonresonant effects can be achieved systematically by expanding the full electroweak theory diagrams of the e^+e^- forward-scattering amplitude according to regions with small $(p_t^2 - m_t^2 \sim m_t \Gamma_t)$ and large $(p_t^2 - m_t^2 \sim m_t^2)$ virtuality in the top and antitop lines [7, 12]. The leading nonresonant contributions are given by two-loop diagrams of order α_{EW}^3 with 3-particle cuts $bW^+\bar{t}$ and $\bar{b}W^-t$, and are suppressed by $\alpha_{\text{EW}}/v \sim v$ (NLO) with respect the leading order (resonant) cross section. The complete set of diagrams can be found in [7]. The EFT power-counting $\alpha_s \sim \alpha_{\text{EW}}^{1/2}$ implies that the NNLO nonresonant corrections arise from (virtual and real) QCD corrections to the NLO diagrams. The number of diagrams at this order exceeds 100, but only the two shown in Fig. 1 contribute to the dominant term in the ρ -expansion, as we explain next.

After integrating over other phase-space variables, the NNLO nonresonant virtual contributions to the to-

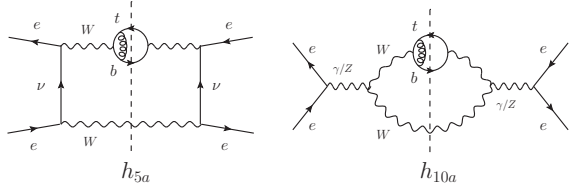


FIG. 2. Example diagrams contributing to the NNLO non-resonant cross section with virtual W -bosons.

tal cross section can be casted in the form [9]

$$\int_x^1 \frac{dt}{(1-t)^{r+n\epsilon}} h(t, x), \quad (1)$$

where the outer integration variable, $t \equiv p_t^2/m_t^2$, corresponds to the invariant mass of the bW^+ subsystem, $p_t = p_b + p_W$, and $x \equiv m_t^2/M_W^2$. The functions $h(t, x)$ contain the result of gluon loop integrals like those of Figs. 1,2, whereas the explicit powers of $(1-t)$ arise from top propagators and phase-space factors (see [9] for details). Since $1-x = \rho(2-\rho)$, the expansion for small ρ can be traded by an expansion in $(1-x)$. Let us first note that the integration domain in (1) implies that $0 \leq 1-t \leq 1-x$. Therefore, the leading terms in $(1-x)$ can be identified by asymptotically expanding the integrand $h(t, x)$ around the phase-space endpoint $t = 1$, i.e. in powers of $(1-t)$, which are transformed into powers of $(1-x)$ upon integration over t . The expansion of the NNLO contributions in the endpoint was carried out in [9] up to terms of order $(\Lambda/m_t)^0 \ln \Lambda$, where the lower limit in the t -integration was limited by $(1-\Lambda^2/m_t^2)$ to regulate the endpoint behaviour. The straightforward replacement $\Lambda^2/m_t^2 \rightarrow 1-x$ into the results of [9] yields that the leading terms scale as $(1-x)^{-1}$ and arise only from diagrams h_{1a} and h_{1b} . Some caution has to be taken with the diagrams involving intermediate W -bosons, since in the limit $\rho \rightarrow 0$ where $M_W \rightarrow m_t$ these become nonrelativistic and their propagator contributes with a factor $1/(m_t^2 - M_W^2) \sim 1/m_t^2(1-x)$ to the amplitude. The NNLO diagrams where this enhancement is most relevant are those of Fig. 2. Taking into account that its endpoint behaviour is $(\Lambda/m_t)^3 \sim (1-x)^{3/2}$ [7], an overall scaling $(1-x)^{-1/2} \simeq \rho^{-1/2}$ is then found for diagram h_{5a} , in agreement with the findings of [1]. Diagram h_{10a} carries a further $(1-x)^2$ suppression factor because s -channel W^+W^- production is suppressed in the non-relativistic limit. We should also note that the endpoint limit taken in [9] assumed that $(1-x) \sim \mathcal{O}((1-t)^0)$ for the asymptotic expansion in powers of $(1-t)$ of diagrams where the bottom propa-

gator¹, $1/(p_b + k)^2$, is part of the gluon loop with momentum k , such as in h_{1b} . For small $(1-x)$, however, we have to consider that $(1-t)$ but also $(1-x)$ are small quantities in the expansion of the bottom propagator, which invalidates the naive use of [9] to infer the scaling in $(1-x)$ for those cases. A careful examination of the regions involved in diagrams with a bottom quark propagator in the loop reveals that this caveat applies only to h_{1b} . Nevertheless, the ρ^{-1} scaling found for h_{1b} with the naive procedure turns out to be correct, as shown below by explicit computation.

III. RESULTS

For consistency with the calculation of the resonant contribution to the cross section, where finite-width divergences are regulated dimensionally, we deal with the infrared endpoint singularities of the nonresonant side using the $\overline{\text{MS}}$ regularization scheme in $d = 4 - 2\epsilon$. The ρ^{-1} terms from diagrams h_{1a} and h_{1b} arise from potential gluon momentum $k^0 \sim \mathbf{k}^2/m_t \sim m_t(1-t)$ running through the QCD loop. In the case of h_{1a} , the leading contribution from the potential region gives a $(1-t)^{-1/2-\epsilon}$ term, while the two top propaga-

tors plus the phase-space factor provide an extra factor $(1-t)^{-3/2-\epsilon}$. A dependence on x only enters through the off-shell top width

$$\Gamma_t(t) = \Gamma_t^{\text{Born}} \frac{(4\pi)^\epsilon \Gamma(1-\epsilon)}{\Gamma(2-2\epsilon)} m_t^{-2\epsilon} t^{-1+\epsilon} \times \frac{1 + 2(1-\epsilon)\frac{x}{t}}{1+2x} \frac{(t-x)^{2-2\epsilon}}{(1-x)^2}. \quad (2)$$

with Γ_t^{Born} the tree-level top decay width. Upon integration over t , powers of $(1-t)$ and $(t-x)$ are converted into powers of $(1-x)$, and the outcome is proportional to $\Gamma_t^{\text{Born}}/(1-x)$, see (3) below. The computation of diagram h_{1b} is more involved, because after expanding the propagators in the loop according to the potential scaling, it still depends on the anti-top and bottom quark three-momenta. Using a Mellin-Barnes representation to perform the $d^d k$ integral we get a result for the integrand in (1) whose pole structure reveals that, unlike the case of h_{1a} , the leading-order term in the asymptotic expansion in the small parameter $(1-x)$ for the t -integration arises from the region $(1-t) \sim (1-x)^2$ [13].

In this way, the contribution of the two diagrams to the hadronic tensor H of the e^+e^- forward-scattering amplitude, as defined in [9], reads

$$H_{1a} = -2 N_\epsilon v_t^L v_t^R (1-x)^{-1-4\epsilon} \frac{2^{2\epsilon} e^{3\epsilon\gamma_E}}{\pi} \frac{\Gamma(2-\epsilon) \Gamma(1/2+\epsilon) \Gamma(1/2-\epsilon)}{\epsilon(1-4\epsilon^2) \Gamma(2-4\epsilon)}, \quad (3)$$

$$H_{1b} = i^{4\epsilon} N_\epsilon v_t^L v_t^R (1-x)^{-1-6\epsilon} \frac{4 e^{3\epsilon\gamma_E} (3-2\epsilon)}{3(1+4\epsilon)(1-6\epsilon)} \frac{\Gamma(4\epsilon) \Gamma(2-\epsilon) \Gamma(1/2+\epsilon) \Gamma^2(1/2-\epsilon) \Gamma(1-4\epsilon)}{\sqrt{\pi} \Gamma(1-2\epsilon) \Gamma(2-2\epsilon) \Gamma(1/2+2\epsilon) \Gamma(1/2-3\epsilon)}, \quad (4)$$

where $N_\epsilon = m_t \Gamma_t^{\text{Born}} N_c C_F \frac{\alpha_s}{4\pi} (\mu^2/m_t^2)^{3\epsilon}$ and μ is the scale introduced in dimensional regularization. $v_t^{L,R}$ are the vector couplings to the photon and Z -boson of the top quarks at the left-hand and right-hand of the diagram, following the conventions of [9]. We

note that both H_{1a} and H_{1b} produce $1/\epsilon$ divergences, which originate at the endpoint. Using the relation between the hadronic tensor contributions and the cross section given in [9], we find for the dominant term in the expansion in ρ of the NNLO nonresonant cross section the result

$$\sigma_{\text{non-res}}^{(2),\rho} = \frac{8\pi\alpha^2}{s} m_t \Gamma_t^{\text{Born}} N_c C_F \alpha_s \left[\frac{Q_t^2}{s} - \frac{2 Q_t v_t v_e}{(s-M_Z^2)} + \frac{v_t^2(v_e^2 + a_e^2)s}{(s-M_Z^2)^2} \right] \times \frac{1}{\rho} \left(\frac{1}{2\epsilon} + \frac{2}{3} - \ln \frac{\rho}{2} + \ln \frac{\mu_{\text{soft}}^2}{m_t^2} + \mathcal{O}(\rho^{1/2}) \right), \quad (5)$$

¹ The components of the (massless) bottom quark momentum read $p_b^0 = |\vec{p}_b| = m_t(t-x)/2 \sim m_t(1-x)/2$ in the top rest frame,

where $p_t = (p_t^0, \mathbf{0})$.

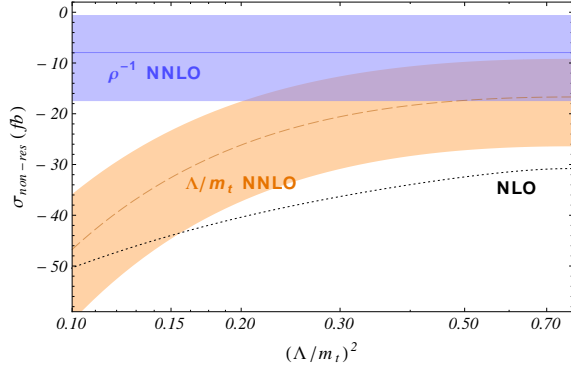


FIG. 3. NNLO non-resonant contribution to $t\bar{t}$ production computed at $s = 4m_t^2$: $1/\rho$ approximation to the total cross section (5) (solid blue line) and first three terms in the Λ/m_t expansion from [9] (dashed orange line), dropping the $1/\epsilon$ and using $\alpha_s \equiv \alpha_s(\mu_{\text{soft}})$ with $\mu_{\text{soft}} = 30$ GeV. The bands show the result of varying μ_{soft} in the interval 15-60 GeV. For comparison, the NLO non-resonant contribution (dotted black line), $\sigma_{\text{non-res}}^{(1)}$ from [7], is also shown.

where we have replaced $\mu^{6\epsilon} \rightarrow \mu_{\text{hard}}^{2\epsilon} \mu_{\text{soft}}^{4\epsilon}$ and taken $\mu_{\text{hard}} = m_t$ because one integration is associated with the hard decay $t \rightarrow bW^+$. The $1/\epsilon$ part of (5) can be shown to cancel against the finite-width divergence $\alpha_s \Gamma_t/\epsilon \times 1/\rho$ in the resonant NNLO cross section, that arises from the insertion of the absorptive matching coefficients $C_p^{(v/a),\text{abs}}$, see Eq. (10) of [9]. Since the latter coefficients were computed at $d = 4$ [6], for a consistent addition of resonant and nonresonant finite pieces, the three-loop resonant diagrams producing these finite-width divergences should also be evaluated in d dimensions².

The size of the NNLO estimate (5) (once the $1/\epsilon$ divergence is removed) is compared to the (exact) NLO result and to the endpoint NNLO approximation with the first three terms in (Λ/m_t) included in Fig. 3. The dependence on μ_{soft} shown in Fig. 3 is compensated by a similar logarithmic dependence as-

sociated to the canceled finite-width divergences in the resonant side. For $\mu_{\text{soft}} = 30$ GeV our estimate for the NNLO non-resonant corrections to the total cross section yields $\sigma_{\text{non-res}}^{(2),\rho} \simeq -8$ fb, representing a $\lesssim 1\%$ negative shift with respect the LO resonant result above the threshold. We note that the extrapolation of the endpoint NNLO approximation for values of Λ close to Λ_{max} approaches the estimate for the total cross section given in this work, although it overestimates its value roughly by a factor of two. The validity of the ρ -expansion at NNLO should be further assessed by computing the next-to-leading order term, of $\mathcal{O}(\rho^{-1/2})$, that gets contributions from a number of sources, some of which have been identified by [1].

Let us finally comment on the result for $\sigma_{\text{non-res}}^{(2),\rho}$ obtained in the latter reference. It is argued in [1] that the nonresonant diagram h_{1b} does not contribute in their framework because it was found to vanish in [14]. The computation of [14] corresponds to a situation where the (potential) gluon momentum $|\mathbf{k}|$ is neglected with respect $m_t - M_W = \rho m_t$ in the phase-space integration of the $t \rightarrow bWg$ subgraph. In the $\rho \rightarrow 0$ limit this simplification is not longer allowed, as we have seen that the dominant term in ρ actually comes from gluon momentum with $|\mathbf{k}|/m_t \sim (1-x) \simeq 2\rho$. To agree with our findings, h_{1b} should also yield a contribution the $\rho \rightarrow 0$ limit in the scheme of [1]. Diagram h_{1b} might also modify the next-to-leading result in ρ given in [1], since it potentially produces sub-dominant terms.

Acknowledgments

I thank B. Jantzen for helpful discussions. This work has been supported in part by the Spanish Government and ERDF funds from the EU Commission [Grants No. FPA2011-23778, No. CSD2007-00042 (Consolider Project CPAN)] and by Generalitat Valenciana under Grant No. PROMETEOII/2013/007.

-
- [1] A. A. Penin and J. H. Piclum, JHEP **1201** (2012) 034.
 - [2] M. Martinez and R. Miquel, Eur. Phys. J. C **27** (2003) 49; K. Seidel, F. Simon, M. Tesar and S. Poss,

Eur. Phys. J. C **73** (2013) 2530; T. Horiguchi *et al.*, arXiv:1310.0563 [hep-ex].

- [3] A. Hoang and M. Stahlhofen, arXiv:1309.6323 [hep-ph].
- [4] M. Beneke, Y. Kiyo and K. Schuller, arXiv:1312.4791 [hep-ph].
- [5] M. Beneke, J. Piclum and T. Rauh, Nucl. Phys. B **880** (2014) 414.
- [6] A. H. Hoang and C. J. Rei  er, Phys. Rev. D **71** (2005) 074022.

² Alternatively, a subtraction scheme that regulates simultaneously the divergences in the resonant and nonresonant parts of the relevant diagrams could be introduced. That analysis is beyond the scope of this note and is postponed to a future publication

- [7] M. Beneke, B. Jantzen and P. Ruiz-Femenía, Nucl. Phys. B **840** (2010) 186.
- [8] A. H. Hoang, C. J. Reiber and P. Ruiz-Femenía, Phys. Rev. D **82** (2010) 014005.
- [9] B. Jantzen and P. Ruiz-Femenía, Phys. Rev. D **88** (2013) 054011.
- [10] M. Beneke and Y. Kiyo, Phys. Lett. B **668** (2008) 143.
- [11] P. Ruiz-Femenía, arXiv:1203.0934 [hep-ph].
- [12] M. Beneke, P. Falgari, C. Schwinn, A. Signer and G. Zanderighi, Nucl. Phys. B **792** (2008) 89.
- [13] This finding has been cross-checked using a MATHEMATICA code to extract poles from Mellin-Barnes integrals written by B. Jantzen.
- [14] K. Melnikov and O. I. Yakovlev, Phys. Lett. B **324** (1994) 217.